(0000) **000**, 000–000

Removing tides from gravity time-series: a comparison of classical methods applied to a global network of superconducting gravimeters

Arthur Valencio[1⋆], Celso Grebogi[1], Murilo S. Baptista[1]

[1] *Institute for Complex Systems and Mathematical Biology, King's College, University of Aberdeen, Aberdeen,* AB24 3UE*, United Kingdom*

28 February 2017

arXiv:1702.08363v1 [physics.geo-ph] 27 Feb 2017

SUMMARY

Many measurements of geophysical interest are contaminated by tidal effects, which can have amplitudes greater than the ones in the events that are intended to be investigated. One of these measurements is the precise monitoring of the gravity field of the Earth, regarded as a powerful tool for investigation of seismically induced deformations, hydrological effects on the ground, ice cap variations, and potential candidate for novel earthquake early-warning systems. Superconducting gravimeters have sensitivity below the $1\ \mathrm{nm\ s^{-2}}$ level, able to investigate those phenomena, and data from instruments in 33 locations globally distributed are available through the International Geodynamics and Earth Tides Service. However, fluctuations due to the Earth tides, with amplitudes typically in the order of few $\mu\mathrm{m\ s^{-2}}$, dominate the signals, and must be removed before proceeding to the specific applications. In this work, we compare, for 5 locations (8 instruments) representative of the network, three different conceptual approaches that could be used for tide removal: frequency filtering, physical modelling and data-based modelling. Each approach applied to gravity time-series has shown a different limitation to be considered depending on the intended application. Results reveal that vestiges of tides remain in the residues for the modelling procedures, whereas the signal was distorted in the filtering procedures. The classical method with the best performance was the least-squares data-based modelling. However, the validation tests were not fulfilled, issue commonly related to overfitting. Although the tides could not be completely eliminated by the methods, they were sufficiently reduced to allow observation of geophysical events of interest above the $10\ \mathrm{nm\ s^{-2}}$ level, exemplified by a hydrology-related event of $60\ \mathrm{nm\ s^{-2}}$. The implementations adopted for each conceptual approach are general, so that their principles could be applied to other kinds of signals affected by tides

Key words: Tidal filtering – Tides – Gravity time-series – IGETS – gravity residuals.

1 INTRODUCTION

Mass displacements induce variations to the gravity field, which allows precise gravity measurements to be used as a tool for investigating polar ice cap variations and melting (Sato et al., 2006), hydrological effects such as remote assessment of underground water reservoirs (Imanishi et al., 2006) and forest evapotranspiration rates (Van Camp et al., 2016), and co-seismic and post-seismic deformations (Imanishi, 2004; Soldati et al., 1998). In addition, there have been recent theoretical proposals relating gravity-field perturbations to propagation of compressional seismic waves, hence opening the possibility for novel early-warning systems able to detect seismic events even before the P-wave arrival (Montagner et al., 2016). Typically the gravity variations at a surface point for the investigation of the mentioned effects are in the order of few $\mathrm{nm\ s^{-2}}$.

The main instrument that can reach $\mathrm{nm\ s^{-2}}$ precision is the superconducting gravimeter, device that replicates the behaviour of an ideal spring by making use of superconducting sphere levitated by the magnetic field from persistent currents in a coil. In such device, changes of local gravity induces changes to the system, and the information is translated to a relative gravity measurement (Goodkind, 1999). The Global Geodynamics Project (GGP) was the first effort of combining globally distributed superconducting gravimeter stations to effectively create a network of these instruments (Crossley & Hinderer, 2009). Currently the project is taken over by the International Geodynamics and Earth Tide Service (IGETS), which makes the data from 33 stations available for research (http://isdc.gfz-potsdam.de/igets-data-base).

The raw gravity signal, however, is dominated by tidal effects, responsible to induce oscillatory behaviour with amplitudes typically in the order of 1000–2000 $\mathrm{nm\ s^{-2}}$, which must be filtered if any of the other geophysical events of interest are to be observed. These tidal effects are not single frequencies in the diurnal, semi-diurnal and terdiurnal values, but several tidal modes around those values, as first systematically studied by the mathematician

⋆ Corresponding author: a.valencio@abdn.ac.uk

sir George Darwin (1907). Despite progress in the development of more complete tidal tables, the Darwin nomenclature for the main tidal modes remains in use (*e.g.* diurnal: K1, O1; semidiurnal: M2, S2; terdiurnal: M3, MK3). Presence of high amplitude tidal signals, masking any events of particular research focus in the frequencies below 5 cycles per day (around $5.79 \cdot 10^{-5}$ Hz), is also present in other signals of interest, such as ground displacement measured by GNSS systems, ground strain and water levels in open and confined systems.

In this paper, we consider three conceptually distinct approaches that can be adopted for removing the tides: (i) frequency filtering of the theoretically predicted components; (ii) physical modelling of the contributing sources to the signal; (iii) and data-based modelling, which analyses the signal itself to adjust the tidal effects at the location. The description of how each method is implemented is described in Sec. 2.2. Although special focus is given to the gravity time-series, the principles from each method can be applied to signals of other nature, provided the necessary necessary adjustments are made. In the results (Sec. 3) it is shown that in terms of eliminating the tides a frequency filtering based on Fourier analysis may be effective. However, a significant consequence is the artificial removal of information near tidal frequencies, which may not be of physical and geophysical interest. A frequency filtering based on a multiband filter is unable to remove all tides, and, additionally, distorts the frequency spectrum. The physical modelling, based on the theoretical simulation of the contributing physical sources to the signal, is only able to reduce the tidal amplitudes, but tidal peaks remain present. The data-based method was considered having the best performance to reduce the gravity residuals, however also in this method the validation conditions are not fully satisfied, which means misfitting are possible to have occurred. The residuals from this method, however, show significant reduction of tides to allow the observation of hydrology-induced gravity changes, which is described in Sec. 3.1.

2 METHODS

2.1 Selected stations

For this study, it were selected the instruments in the locations of Sutherland in South Africa (SU, 3 instruments), Schiltach/Black Forest in Germany (BF, 2 instruments), Ny-Ålesund in Svalbard island, Norway (NY, 1 instrument), Matsushiro in Japan (MA, 1 instrument), and Apache Point in New Mexico, USA (AP, 1 instrument), distributed according to Fig. 1. The data period available for this study and type of each instrument producing the time-series are detailed in Table 1. The chosen instruments are a representative sample of the differences of stations in IGETS network, including different latitudes, different site conditions (*e.g.* continentality, vegetation, climate conditions, etc), and different generations of gravimeter instruments. For this analysis it was used 1-min sampling time-series data. Example of time-series and frequency spectrum are shown in Fig. 2.

2.2 Tidal removal methods

2.2.1 Pre-processing

Although local operators provide the IGETS users with data corrected for spikes and clippings related to the helium refill procedure or to strong motions in the location, the time-series still contain data gaps, offsets and instrument linear trends, which must

Figure 1. Location of the IGETS superconducting gravimetry stations. The locations of the stations used for this study are presented in black squares. Gray circles represent the other IGETS stations with data currently available to users

Table 1. Instruments and period of the datasets used in this study

Instr.	Gravimeter type	Data period
AP	Observatory SG (3rd gen)	01/Jan/2009 to 31/Dec/2015
BF1	Observatory SG (3rd gen)	01/Oct/2009 to 31/Dec/2015
BF2	Observatory SG (3rd gen)	01/Oct/2009 to 31/Dec/2015
MA	"Tidal" SG (1st gen)	01/Jul/1997 to 30/Jun/2008
NY	Compact SG (2nd gen)	20/Sep/1999 to 31/Jan/2012
SU1	Compact dual-sphere SG (2nd gen)	27/Mar/2000 to 31/Dec/2015
SU2	Compact dual-sphere SG (2nd gen)	30/Sep/2000 to 31/Dec/2015
SU3	Observatory SG (3rd gen)	01/Sep/2008 to 31/Dec/2015

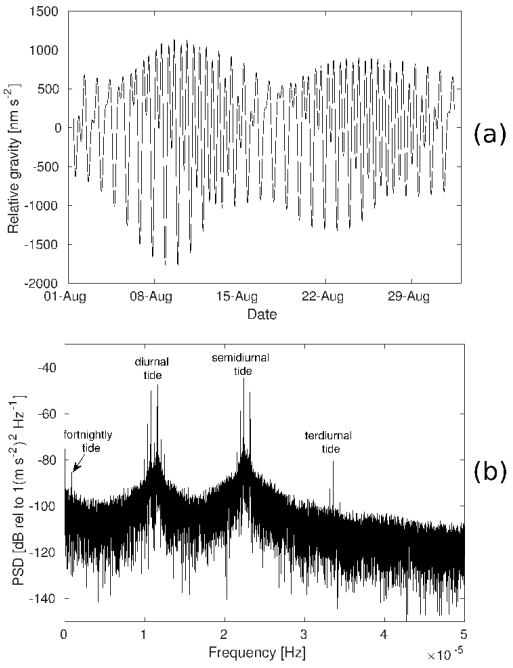

Figure 2. Example of gravity signal from the SU3 instrument, in South Africa. Top panel: 1 month sample (August 2010) of the relative gravity measurements. Bottom panel: Power spectrum density of the time-series. Diurnal, semi-diurnal and terdiurnal tides are particularly evident, as indicated. Fortnightly tide can also be observed as a long-period modulation of the time-series or a line in the frequency domain.

be considered prior to the application of the tidal removal methods. Also the contribution of the atmospheric mass to the gravity signal must be accounted. The three classes of methods considered for tidal removal, frequency filtering, physical modelling and data-based modelling, have different demands of pre-processing. In the case of frequency filtering, data gaps cannot be present, hence missing intervals, which can be as large as many months, must be temporarily replaced with a synthetic gravity signal. Regardless of that, 90% of the local atmospheric contribution to gravity can be removed by considering a linear proportion between the atmospheric gravity variation (δg_{atm}) and the air-pressure change (δp), with the proportionality constant (atmospheric admittance) being $\alpha = \delta g_{atm}/\delta p = -3.56$ [nm s^{-2}mbar^{-1}] (Merrian, 1992), which is considered a sufficient atmospheric correction for this method. The physical modelling and data-based modelling procedures do not require filling the gaps in the time-series, and use a more complete analysis for atmospheric contribution, thus being sufficient to only correct for offsets and instrument linear trends on the pre-processing. This was performed with a semi-automatic implementation of the remove-restore procedure (Hinderer et al., 2015, p.81) on Matlab.

2.2.2 *Frequency filtering*

This filtering method consists of simply removing the undesirable tidal frequencies. It is mainly adopted as a preliminary analysis of the spectrum or for the investigation of low-frequency seismic modes known to be out-of-resonance with tides. The tidal frequencies were obtained from the Tamura (1987) tables, containing 1200 constituent waves. These frequencies may be removed from the original gravity signal either in the time-domain or frequency-domain. For the time-domain it was applied a multiband finite-impulse response (FIR) filter with zero-phase distortion, and for the frequency domain it was adopted the classical procedure of analysing the Fourier spectrum, removing the selected frequencies, and reconstructing the time-series by inverse Fourier transform. Original gaps were reintroduced in the residuals, and extra gap margins of 1-week before and after the original gaps were included to remove artificial ringing effects (Gibbs phenomenon). It must be stressed that these procedures for obtaining the gravity residuals are not suitable for all applications. In particular applications involving signals close to resonance with tides or investigation of very broad-band events should not adopt this method. It is also not recommended for studies that require the quantification of informational measures in the time-series, since this method artificially removes information from the data.

2.2.3 *Physical modelling*

This method is based on modelling all the known tidal gravity contributions from astronomical and planetary effects, resulting in a theoretical prediction. Such prediction is then subtracted from the observed signal so to obtain the gravity residuals, which would only contain the events of interest, such as co-seismic changes. Therefore it is required to properly select the other phenomena that produces gravity changes, and to consider how they are described. For this study it was considered the following effects: solid Earth tides, ocean tidal loading, atmospheric gravity contribution, ocean non-tidal loading, hydrology loading and polar tides.

The solid Earth tides, also referred as body tides, are the direct effects of the gravitational pull of astronomical objects over either a homogeneous or layered Earth model, resulting in ground displacements in the order of tenths of cm and local gravity changes in the order of μm s^{-2}. This is calculated through a tide generating potential $V_{SE}(\boldsymbol{r}, t)$ of the form of equation (1) (Agnew, 2007), with (r,θ,ϕ) specifying the location (radial distance, co-latitude, longitude), g_e the mean gravity of the Earth at the equator, Y the spherical harmonics, and $c_{lm}(t)$ the complex coefficients calculated from the attraction of the astronomical bodies, which are typically computed from an harmonic expansion. To such Earth model it is then subsequently added the contribution of the oceans, which changes gravity due to the direct mass movement but also deforms back the ground due to the significant weight of water being periodically redistributed. This effect is the ocean tidal loading, computed from a tidal generating potential such as $V_{OL}(\boldsymbol{r}, t)$ given by equation (2) (Farrell, 1973), with ρ the density of water, $H(\boldsymbol{r}')$ the tide at the ocean in the location r', and $G(|\boldsymbol{r} - \boldsymbol{r}'|)$ the Green's function for the distance, which appears as solutions for the elastic and Poisson equations of a layered Earth. The gravity tide is obtained from the generating potentials by taking the derivative in the radial direction. The work of Farrell (1972) describes how the tide generating potentials can also be applied to measurements of tidal displacements, tilts, or strain, and, in addition, exemplifies how the Green's function used can be obtained from first principles for a layered Earth model. Both the ocean tidal loading and the solid Earth tides were computed for the selected stations using the software ATLANTIDA3.1_2014 (Spiridonov et al., 2015), with the assumptions of tidal periodicities following the Tamura (1987) tables, layered Earth model IASP91, and ocean model FES2012.

$$V_{SE}(\boldsymbol{r}; t) = g_e \,\mathrm{Re}\left[\sum_{n=2}^{\infty}\sum_{m=1}^{n} c^*_{nm}(t) Y_{lm}(\theta, \lambda)\right] \tag{1}$$

$$V_{OL}(\boldsymbol{r}; t) = \rho \iint_{\mathrm{ocean}} G(|\boldsymbol{r} - \boldsymbol{r'}|) H(\boldsymbol{r'}) dS \tag{2}$$

Mass redistribution in the atmosphere also causes significant gravity variations, up to the order of 100nm s^{-2}. Analogously to what occurs with the ocean tidal loading, the atmospheric mass redistribution leads to fluctuations on the surface of ground and oceans, in particular with the oceans responding as an inverted barometer for periods larger than one week. Although the atmospheric contribution is dominated by the local admittance, based on reading the air pressure at the station, a full description involves computing local and non-local air mass displacements. There are two services providing numerical results of atmospheric gravity based on finite element models: Atmospheric Loading service, provided by EOST/University of Strasbourg (http://loading.u-strasbourg.fr/sg_atmos.php), and ATMACS, provided by BKG (http://atmacs.bkg.bund.de). For this study it has been adopted the first, selecting the atmospheric data provided from ECMWF ERA-Interim reanalysis (http://www.ecmwf.int/en/research/climate-reanalysis/era-interim), which is able to cover the entire gravity time-series period for all stations. The data, however, is sampled in 6h, and interpolation is necessary.

The ocean non-tidal loading refers to other changes in the water mass due to circulation of currents and wind forcing. These lead to gravity changes that can be larger than ocean tidal loading. Theoretical predictions are calculated similarly to the atmospheric loading, but using the ocean bottom pressure data from the ECCO2 model (http://ecco2.jpl.nasa.gov/). Similar procedure is adopted for the calculation of hydrology loading con-

tributions, due to soil moisture changes, where again it was selected weather data from ERA-Interim reanalysis. Services providing the numerical results using such models for all stations are available from EOST/University of Strasbourg (http://loading.u-strasbg.fr/sg_ocean.php, http://loading.u-strasbg.fr/sg_hydro.php).

Finally, the polar tides are a result of the Chandler wobble, small variation of Earths axis of rotation. Using the Earth Orientation data EOPC04 from the International Earth Rotation Service (ftp://hpiers.obspr.fr/iers/eop/eopc04), the polar tides can be calculated as $\delta g_{polar} = -39 \times 10^6 \sin 2\theta (m_1 \cos\lambda + m_2 \sin\lambda)$ [nm s^{-2}], with (θ, λ) again the co-latitude and longitude of the station, and (m_1,m_2) the equivalent (x,y) polar motion amplitudes converted to radians (Wahr, 1985).

Figure 3 exemplifies the scale from each contribution and procedure for tidal signal removal. A detailed review of these processes can be found in Crossley et al. (2013), Hinderer et al.(2015) and Boy and Hinderer (2006). The input parameters for physical modelling are referent only to the station location and local/global conditions, and no *a priori* information of the gravity time-series is used. Advantages of this method are the maintenance of information produced on all frequency bands provided by the device, and the possibility of clearly defining the physical origin of any given contribution, including control to maintain aspects of interest according to the application. For example, it is of interest to maintain hydrology loading when the objective of the research is to investigate the gravity response to rainfall, evapotranspiration and aquifer recharge, but still all other contributions should be removed. The limitation in the method is that misfitting in the models introduces undesirable fluctuations to the residuals. Figure 3 (h) makes this evident by the oscillatory pattern with semi-diurnal frequencies. Spectral analysis identifies these oscillatory frequencies in the residuals as corresponding to the tidal modes M2, S2 and K2.

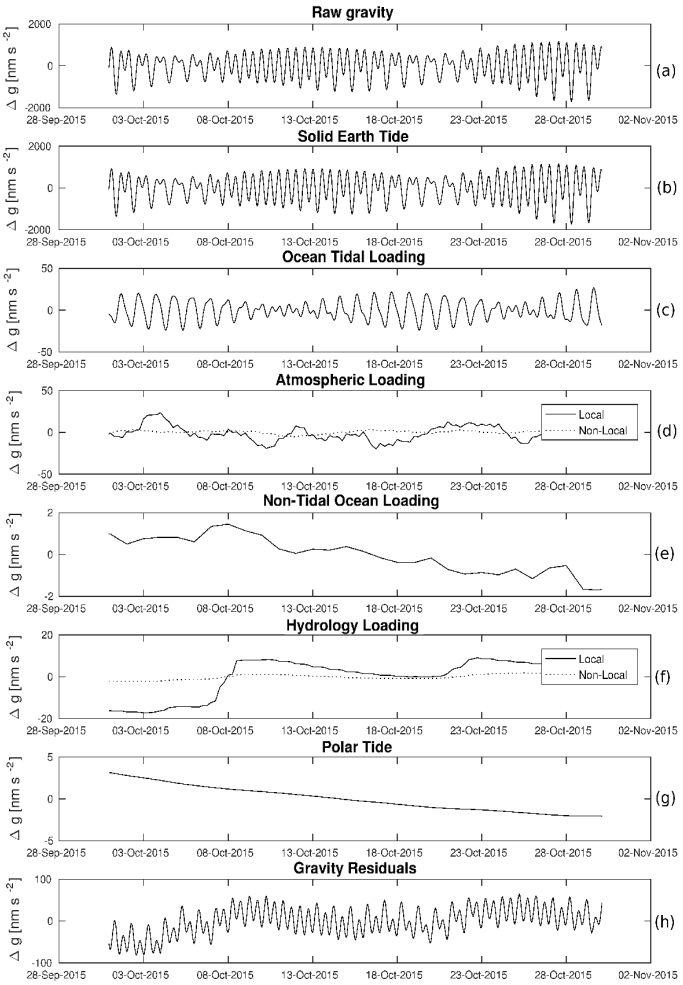

Figure 3. Example of physical modelling applied to 1-month data sample (October 2015) of AP instrument (New Mexico). The gravity residuals (h) are obtained by subtracting the measured relative gravity (a) by all the following simulated contributions: solid Earth tide (b), ocean tidal loading (c), atmospheric loading (d), non-tidal ocean loading (e), hydrology loading (f) and polar tide (g). In this sample, there was a misfitting of the amplitudes of the theoretical semidiurnal tides with the observations, so oscillations are still present in the gravity residuals (h), albeit with smaller amplitude than in the original time-series (a).

2.2.4 Data-based modelling

In the previous method the theoretical prediction of tidal mode amplitudes from solid Earth tides and ocean tidal loading was based on a tide generating potential model using only information of location of the instrument and initial time of the dataset as inputs. The tidal modes that remained in the residuals of Fig. 3 (h), however, are strongly associated with these two physical origins, meaning that the theoretical model of these tidal components does not completely fit with the observations at the station. A way of overcoming this is to analyse the regularities in the gravity data itself, extracting from the data the suitable tidal coefficients to the station location. The usual approach is the classical harmonic or least-square fitting, based on defining amplitudes and phases to sinusoids of tabled tidal frequencies, in such a way that the sum of the square of the residual values is minimised. For compatibility, the Tamura (1987) tables are again adopted to provide the tidal frequencies. Recent tools developed for oceanography, such as UTide (Codiga, 2011), have included a series of optimisations, being able to account for data gaps and long time-series without issues, and can be easily adapted to gravity data. The table of data-based tidal constituents is then used to reconstruct only the tidal part of the time-series, and the difference with the observation provides the residue. Two issues arise with this method. The first is the errors-in-variables problem highlighted by Kantz and Schreiber (1997, p.218) and Agnew (2007): misfitting occurs in the presence of non-white noise, and the noise profile of the gravity time-series exhibits redness (*i.e.* varies with frequency approximately on f^{-2}). The second issue is that noise factors or other geophysical events of potential interest might have important components near tidal frequencies, and the procedure will mistakenly consider these as part of the contribution of the tidal constituent, hence a type of overfitting. Sophisticated programs deal with these specific issues in a number of ways. We have not incorporated in this study incremental developments specifically tailored to gravity, as our intention is to compare different general methodological approaches to tidal removal, able to be also applied to other signals such as displacement, tilt, strain and water levels. I.e., we have not adopted implementations such as the ETERNA package (Wenzel, 1996), VAV/2000 (Venedikov et al., 2001), and BAYTAP08 (Tamura & Agnew, 2008) in this study. The main underlying principle in these programmes remain the least-squares technique (in modified versions), and a comparison of their implementation and performance was done by Dierks and Neumeyer (2002). Additionally, the least-squares procedure was tailored to fit only the tidal frequency contributions. Hence, non-tidal effects, such as polar motion, atmospheric loading, hydrology loading and

ocean non-tidal loading, must still be removed following the same sequence described in the physical modelling.

3 RESULTS

Once the residuals from each method have been obtained, it is of interest to observe if the tides were eliminated by analysing the frequency spectra. Fig. 4 shows the Lomb-Scragle power spectral density of the residuals for the BF1 instrument, in Schiltach/Black Forest, Germany. This type of power spectrum calculation, computed from equation (3), is preferred over other types of periodogram for its direct applicability to data with large gaps (Scragle, 1982), such as the gravity time-series. In the expression, x_i are the data points at times t_i, and have the average and variance given by $\bar{x}$ and σ^2; the constant τ is only a time offset that ensures time-invariance during computation. Figures 4 (d) and (e) show that the diurnal, semidiurnal and terdiurnal tides are still present after filtering with the physical modelling and data-based modelling methods. The amplitude of the semidiurnal tides are slightly larger in the physical modelling case, whereas the data-based modelling reveals larger terdiurnal constituents. However in both cases the highest tidal peaks were reduced below the New Earth High Noise Model (NHMN) reference line, and some tidal constituents, especially the diurnal (around $1.16 \cdot 10^{-5}$ Hz), went also below the New Earth Low Noise Model (NHMN) (Peterson, 1993). Frequency filtering (Figs. 4 (b) and (c)) were able to eliminate the diurnal and semidiurnal tides, as well as the FIR filtering. The effect of the Fourier filtering in deleting the tidal frequencies is evident in Fi. 4 (b), with considerable frequency gaps where information is lost. The FIR filtering proved more adequate, once it was implemented to strongly damp the tidal frequencies instead of deleting them. However, due to limitations of design (constrained by the highest order possible to obtain and apply to data), it produced artificial distortions in regions around $0.5 \cdot 10^{-5}$ Hz, $3.2 \cdot 10^{-5}$ Hz and $4.4 \cdot 10^{-5}$ Hz, while a terdiurnal tide (M3) remained present $3.4 \cdot 10^{-5}$ Hz. The more precise modelling of the atmospheric contribution adopted in the physical and data-based modelling have significantly reduced the power of the residuals over the whole range of frequencies plotted. That is revealed by the drop in the base (noise) level in Fig. 4 (d) and (e) compared to (b) and (c). Due to this, the quaterdiurnal tides, which typically are not observable for their small amplitude compared to background noise, expressed visible peaks at $4.6 \cdot 10^{-5}$ Hz in Figs. 4 (d) and (e). The spectral results for other stations are similar, with few specificities relating to site conditions; the plots are available in the Supplementary Material.

$$P(f) = \frac{1}{2\sigma^2}\left\{ \frac{\left[\sum_{i=1}^{N} x_i - \bar{x}\cos\left(2\pi f(t_i-\tau)\right)\right]^2}{\sum_{i=1}^{N}\cos^2(2\pi f(t_i-\tau))} + \frac{\left[\sum_{i=1}^{N} x_i - \bar{x}\sin\left(2\pi f(t_i-\tau)\right)\right]^2}{\sum_{i=1}^{N}\sin^2(2\pi f(t_i-\tau))} \right\} \quad (3)$$

As the power spectrum indicates that tidal components remain in the residuals, the amplitude levels of the tidal constituents in the residuals were calculated from classical harmonic analysis, with the main observed modes shown in Table 2. For the Fourier filtering method (FFT), the results confirm that the main peaks were largely eliminated, with largest modes appearing being consistent with noise. The finite-impulse response (FIR) filtering, though, consistently was not able to filter the terdiurnal tides, with the main

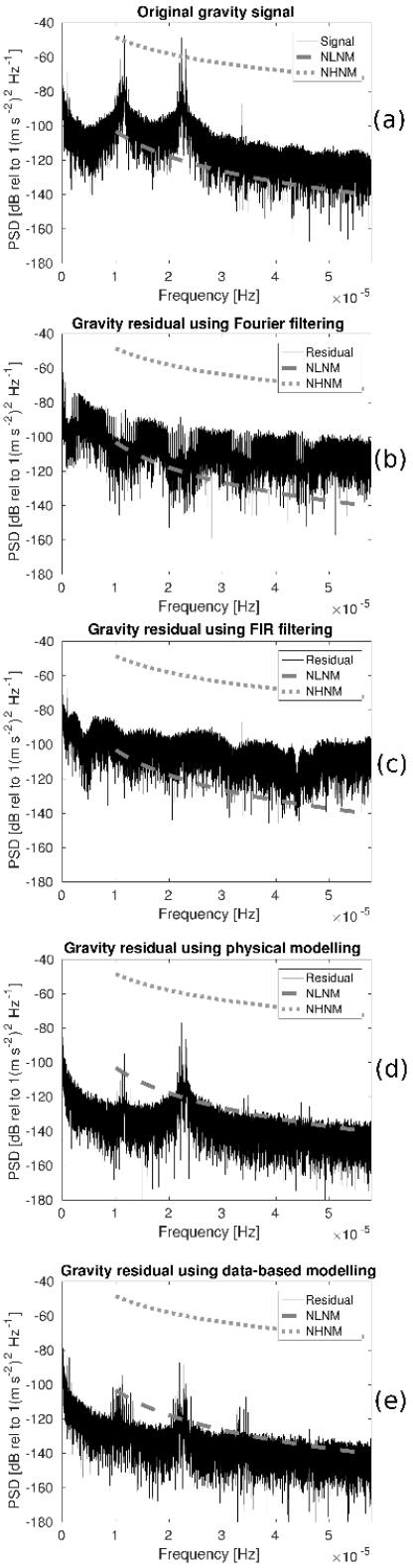

Figure 4. Lomb-Scragle power spectral density of the original gravity signal (a) and gravity residuals (b-e) from BF1 instrument, Schiltach/Black Forest, Germany, as obtained from the different methods of tide removal: Fourier filtering (b), FIR filtering (c), physical modelling (d), and data-based modelling using least squares (e). For reference, the New Earth Low Noise Model (NLNM) and the New Earth High Noise Model (NHNM) are indicated. Results for other stations are provided in the Supplementary Material.

mode (M3) appearing to even have a small gain, which reveals a issue with the filter design. The physical modelling (PM) was able to eliminate the terdiurnal components, but it remained with noticeable amplitudes in the important diurnal (K1,O1,S1) and semidiurnal (M2,S2,K2) modes, despite reductions above 90% in the levels of the greatest peaks. Except from rare occasions possibly related to instrument site conditions, the least-squares data-based modelling (LS) was able to reduce the main peaks to levels below 2 nm s^{-2}, with the largest peak typically not being the original largest mode but a neighbour.

A further inquiry is whether the energy in the observed peaks components change in time or remain constant. If it changes, the observed peak in the spectrum might be the result of a temporary effect, of non-tidal origin. For example, the occurrence of earthquakes of large magnitude could induce vibration modes in the tidal region (Slichter triplet, core modes), but these would have well defined start-end times for the energy release, in opposition to tides, which would be continuous throughout the time-series. The spectrogram of the residuals (Fig. 5) shows, however, uniformity in these frequency contributions along the time, as indicated by the arrows (vertical dark regions are due to time-series gaps). In line with the tidal hypothesis, the cross-correlation between the residuals and the theoretical tides (Fig. 6) is particularly high at all time lags with the physical modelling residuals (d). However, the residuals from other methods had low correlation with theoretical tides [Fig. 6 (b), (c) and (e)], with value below the comparative margins from a red-noise model for gravity residuals. These correlation results reinforce the observation from Table 2 that the physical modelling residuals remain with significant components of the main tides, whereas the residuals from the other methods removes the main tides but maintain the smaller ones.

The data-based method produced the best results for tidal filtering without canceling other frequency information. However, the method requires the assumptions of independence and normality of the residuals. Bezruchko and Smirnov (2010, pp.222-225) considered that the independence can be tested by the autocorrelation function and the normality by the histogram. The AP instrument results indicate that independence (Fig. 7 (a)) and normality (Fig. 7 (b))cannot be validated. The autocorrelation function produced non-conclusive results similar to the red noise hypotheses. The histogram diverged both from the white and red noise profiles, though. Similar mismatch occurs across all instruments. It means that the data-based model employed was not able to fully describe the series and may have incurred in misfitting of frequency component amplitudes, which explains the still observed oscillations in the residual time-series, generally lower than 100 nm s^{-2} total amplitude in the time-series.

Finally, Table 3 shows the correlation between residuals obtained through different methods. Correlation between physical and data-based modelling residuals (column 3) is typically high except for the station in Matsushiro (MA), Japan, and two instruments in Sutherland (SU), South Africa. For MA the local seasonal effects, particularly from atmospheric and ocean events, provides a difficult scenario for the physical modelling, specifically in fitting the diurnal tidal components particular to this station. However, the data-based residuals can adjust better to this case, leading to a lower correlation. The cases of SU2 and SU3 should also be considered in the light of local conditions and agreement with theoretical models. High correlation in other stations reveals the methods of physical and data-based modelling tend to converge. The correlation between the two types of frequency filtering, by contrast, is low in all

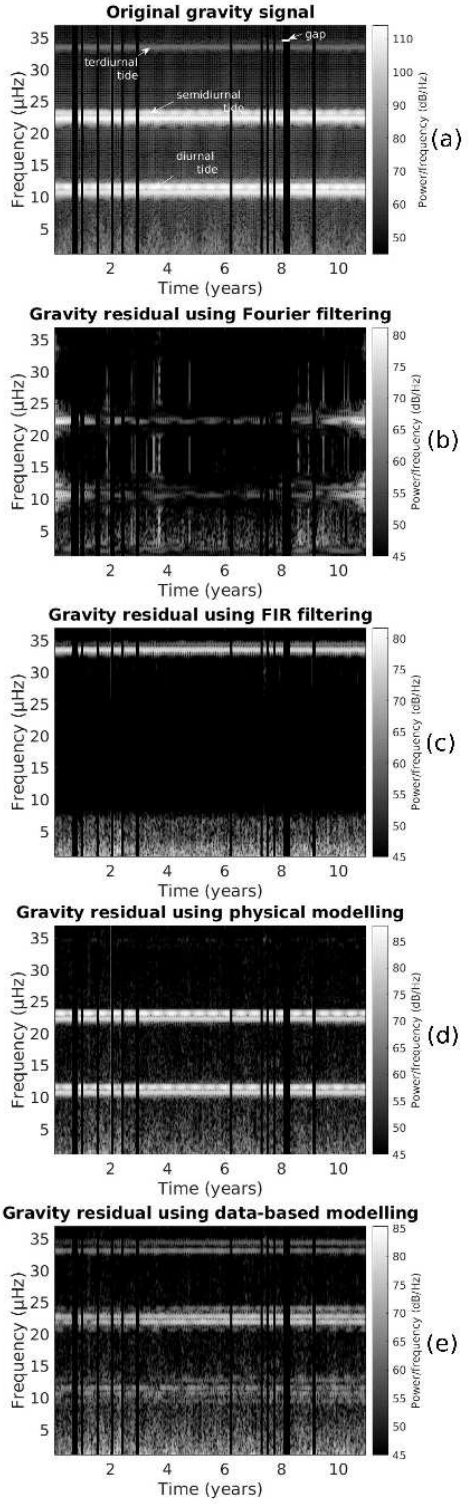

Figure 5. Spectrogram in the range of the main tidal frequencies of the original signal (a) and the residuals (b-e) for the MA instrument, Matsushiro, Japan. The frequency areas of higher energy present in the residuals coincide with the main tidal regions identified in the original gravity signal. Also, these areas of higher energy remain almost constant throughout the whole time-series, as expected from tides. If the cause for the higher energy signals were events localised in time, such as seismic phenomena, the spectrogram would show the energy peaks with well defined start and end times, which is not observed. The pattern is analogous for the other stations. Vertical dark regions are data gaps.

Table 2. Amplitudes of the main diurnal, semidiurnal and terdiurnal tidal components of original gravity series (column 3) and residuals [nm s^{-2}] (columns 4-7), for each station (column 1). Confidence levels and tidal group are indicated in parentheses. Numbers in bold show high amplitude tidal peaks remaining in the residuals.

Inst.	Tidal component	Original series	FFT residual	FIR residual	PM residual	LS residual
AP	Largest diurnal	457.52(0.06)(K1)	0.8(0.3)(S1)	0.7(0.1)(Q1)	**13.81(0.05)(K1)**	0.53(0.05)(S1)
	Largest semidiurnal	616.3(0.2)(M2)	0.3(0.1)(MKS2)	0.3(0.4)(M2)	**19.4(0.2)(K2)**	0.6(0.1)(S2)
	Largest terdiurnal	9.42(0.05)(M3)	0.43(0.09)(SK3)	**9.84(0.05)(M3)**	0.12(0.01)(MK3)	0.14(0.05)(SK3)
BF1	Largest diurnal	493.37(0.08)(K1)	1.3(0.4)(BET1)	0.15(0.06)(S1)	**2.09(0.03)(K1)**	0.45(0.08)(S1)
	Largest semidiurnal	394.0(0.1)(M2)	0.8(0.2)(NU2)	0.04(0.02)(H2)	**15.9(0.1)(M2)**	1.0(0.1)(S2)
	Largest terdiurnal	4.60(0.02)(M3)	0.3(0.2)(M3)	**4.88(0.03)(M3)**	0.05(0.01)(MK3)	0.16(0.02)(MO3)
BF2	Largest diurnal	493.37(0.08)(K1)	1.0(0.4)(BET1)	0.275(0.08)(2Q1)	**2.24(0.02)(K1)**	0.52(0.08)(S1)
	Largest semidiurnal	394.1(0.1)(M2)	0.6(0.2)(NU2)	0.07(0.02)(MU2)	**15.9(0.1)(M2)**	1.1(0.1)(S2)
	Largest terdiurnal	4.63(0.03)(M3)	0.2(0.1)(MO3)	**4.89(0.03)(M3)**	0.07(0.01)(MK3)	0.16(0.03)(SK3)
MA	Largest diurnal	494.4(0.1)(K1)	0.04(0.03)(TAU1)	0.5(0.4)(2Q1)	**18.24(0.09)(K1)**	**3.3(0.1)(S1)**
	Largest semidiurnal	577.8(0.3)(M2)	0.11(0.03)(NU2)	0.3(0.2)(GAM2)	**16.2(0.3)(M2)**	1.0(0.3)(S2)
	Largest terdiurnal	8.46(0.09)(M3)	0.009(0.007)(SK3)	**8.69(0.09)(M3)**	0.26(0.05)(SK3)	0.31(0.08)(SK3)
NY	Largest diurnal	189.6(0.01)(K1)	0.14(0.03)(S1)	**3(1)(S1)**	**4.22(0.08)(O1)**	0.22(0.09)(S1)
	Largest semidiurnal	21.59(0.05)(M2)	0.02(0.01) (MU2)	0.6(0.6)(S2)	**6.32(0.05)(M2)**	0.18(0.04)(S2)
	Largest terdiurnal	0.20(0.02)(MO3)	0.01(0.01)(MK3)	0.2(0.2)(SO3)	0.24(0.02)(MO3)	0.02(0.02)(SK3)
SU1	Largest diurnal	448.27(0.05)(K1)	0.04(0.02)(S1)	0.2(0.3)(S1)	**3.85(0.03)(S1)**	1.43(0.05)(S1)
	Largest semidiurnal	619.8(0.2)(M2)	0.05(0.04)(H1)	0.1(0.1)(L2)	**54.7(0.3)(M2)**	**2.0(0.2)(S2)**
	Largest terdiurnal	9.28(0.05)(M3)	0.005(0.007)(MK3)	**9.77(0.06)(M3)**	0.277(0.007)(M3)	0.29(0.05)(SK3)
SU2	Largest diurnal	448.30(0.05)(K1)	0.03(0.02)(O1)	0.2(0.2)(S1)	**3.85(0.02)(S1)**	1.43(0.05)(S1)
	Largest semidiurnal	619.9(0.2)(M2)	0.02(0.02)(MSN2)	0.14(0.09)(M2)	**54.8(0.02)(M2)**	**2.0(0.2)(S2)**
	Largest terdiurnal	9.29(0.05)(M3)	0.001(0.004)(OQ2)	**9.78(0.09)(M3)**	0.282(0.007)(M3)	0.29(0.06)(SK3)
SU3	Largest diurnal	448.30(0.09)(K1)	0.5(0.1)(BET1)	0.4(0.6)(NO1)	**3.72(0.05)(S1)**	1.50(0.09)(S1)
	Largest semidiurnal	619.9(0.2)(M2)	0.5(0.2)(NU2)	0.4(0.3)(S2)	**52.9(0.3)(M2)**	**2.0(0.2)(S2)**
	Largest terdiurnal	9.25(0.07)(M3)	0.03(0.02)(SK3)	**9.8(0.2)(M3)**	0.28(0.01)(M3)	0.29(0.08)(SK3)

Table 3. Correlation (Pearson) between the residuals obtained with the FFT and FIR filtering methods (column 2) and with the physical and data-based modelling methods (column 3) for each station (column 1)

Instrument	Correlation between FFT and FIR filtering	Correlation between physical and data-based modelling
AP	-0.0092	0.3152
BF1	-0.0136	0.1403
BF2	-0.0174	0.1159
MA	-0.0024	-0.0191
NY	-0.0246	0.2383
SU1	-0.0020	0.1085
SU2	-0.0060	0.0347
SU3	0.0007	0.0227

cases. The presence of the terdiurnal tide in the FIR residuals is a strong factor contributing to this result.

3.1 Example of application and properties of the residual

Although the tides and large seasonal effects remain present in the residuals from the physical and data-based modelling, their overall amplitudes in the time-series have reduced considerably from the 2000nm s^{-2} level to the 100nm s^{-2} and 10–50nm s^{-2} levels, respectively. These levels enable, for example, the observation of hydrology-induced gravity variations in the time-series. For the MA station (Matsushiro, Japan), Imanishi et al. (2013) describes a theory of these hydrology-induced variations, consisting of a sharp drop in the order of tenths of nm s^{-2} for the gravity measurements during heavy precipitation events, and a slow increase of gravity in the subsequent dry weeks at rates associated to evapotransporation and water infiltration phenomena. Figure 8 reveals this behaviour during the summer of 2002, where the gravity variations in the order of 60nm s^{-2} are associated to intense rainfall in the first weeks of July and relative dry weeks in the period afterwards. This could only be observed with the residuals of data-based modelling, where the remaining tidal amplitudes situated around 20nm s^{-2} for this station in this period. The same phenomena could not be verified in the time-series of the residuals from physical modelling due to larger amplitude oscillations still present (100nm s^{-2}), which mask the event. Co-seismic and post-seismic gravity changes could not be observed yet at this resolution, yet the sensitivity level required (0.1–50nm s^{-2}) is very close.

4 CONCLUSION

This work has discussed three conceptually different approaches to filter tides in a general geophysical time-series, and classical implementations were applied to signals from a network of superconducting gravimeters. These signals in particular exhibit oscillations with amplitudes in the order of 2000nm s^{-2} of tidal origin, while, comparatively, the sensitivity of the instruments is of the order of 0.1–1nm s^{-2}. There is a desirable application of the residuals of these gravity signals after tidal removal for the investigation of events on the nm s^{-2} scale, such as the co-seismic gravity changes (order of $0.1 - 10$ nm s^{-2} day^{-1}), gravity changes due to post-seismic deformations (order of 50 nm $s^{-2}$$month^{-1}$), gravity changes from an incoming compressional seismic wave

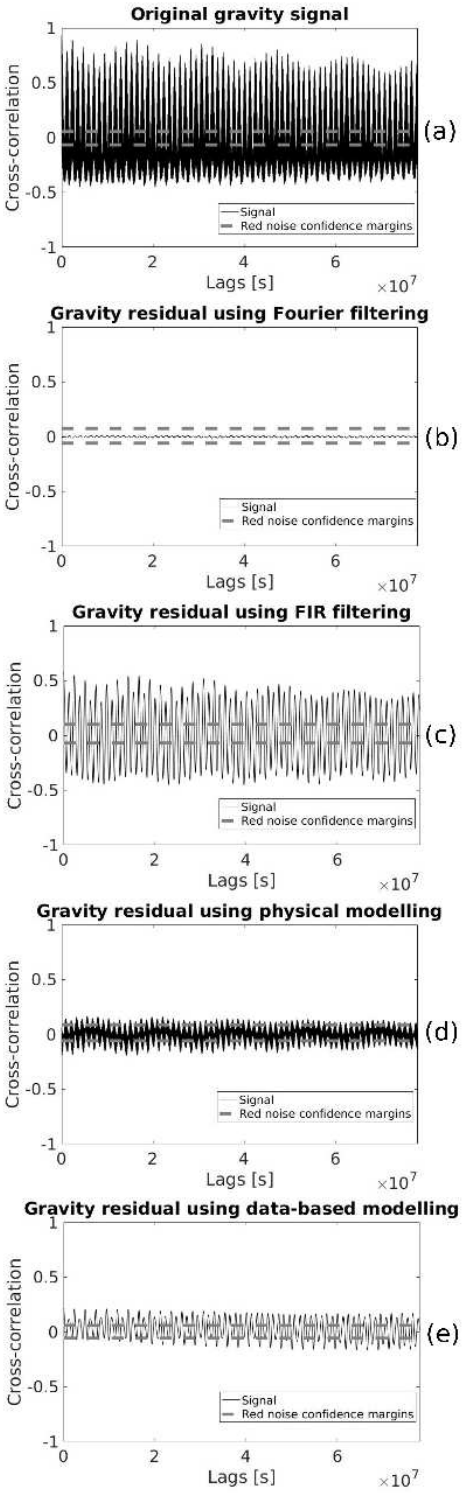

Figure 6. Cross-correlation of original signal (a) and residuals (b-e) with tides on NY instrument, Svalbard island (Norway). Dashed gray lines show confidence margins from correlation between an equal amplitude red noise with the local tides. The maxima of correlation are significantly reduced in comparison with the original signal, particularly with the residuals from Fourier filtering (b), physical modelling (d) and data-based modelling (e) at comparable or lower levels than the correlation from a red noise model. FIR filtering was the only case where correlation with tides remained high for this station.

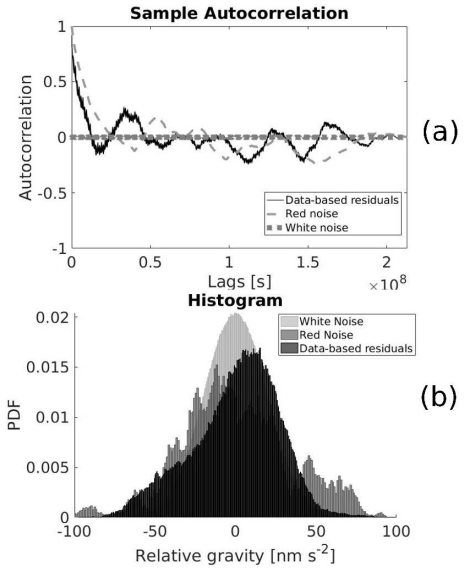

Figure 7. Tests for independence, using sample autocorrelation (a), and normality, using histogram (b), of the data-based residuals from the AP instrument, Apache Point (New Mexico). The results were inconclusive, as the autocorrelation (a) approached red noise behaviour (independence of variables not fully verified) and the histogram also did not fit with the normality condition from white noise. The tests are also inconclusive for the other stations.

(order of 1 nm $s^{-2}s^{-1}$), and hydrological effects (order of $10 - 50$ nm $s^{-2}month^{-1}$). Of the three methods adopted here for removing the tides, the frequency filtering artificially distorted the signal (whether if implemented as Fourier filtering or as a time-domain filter), and both the physical and data-based modelling methods were not able to completely eliminate these oscillations, but could reduce them significantly. In the time-series, the frequency filtering residuals presented typically periodic/quasi-periodic ampli-

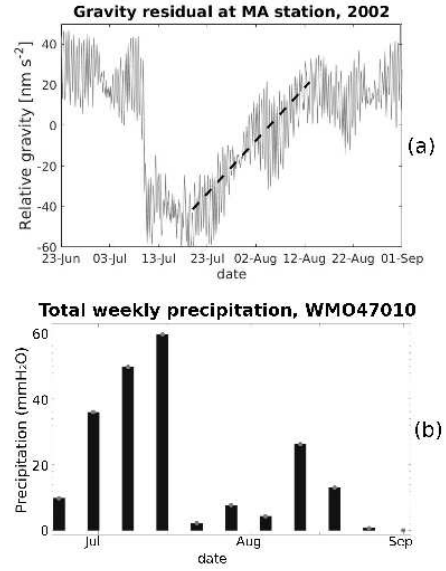

Figure 8. Observation of gravity drop in Matsushiro station associated with peak of precipitation and monthly drift associated to evapotranspiration and water in infiltration. The observation follows model in Imanishi et al (2013). Pluviometric data from nearby meteorological station in Nagano city, Japan.

tudes of the oder of $10\ \mathrm{nm\ s^{-2}}$ with FFT frequency filtering and $50\ \mathrm{nm\ s^{-2}}$ with FIR frequency filtering, but caused significant artificial changes to the frequency spectrum of the signal. Alternative procedures of physical modelling and least-squares data-based modelling generated residuals with quasi-periodic amplitudes in the time-series generally in the order of $100\ \mathrm{nm\ s^{-2}}$ and $10 - 50\ \mathrm{nm\ s^{-2}}$, respectively. The data-based residuals reached enough sensitivity to monitor hydrology-related gravity changes in MA station (Matsushiro, Japan) in the order of $60\ \mathrm{nm\ s^{-2}}$, and could also be applied to observation of any other phenomena above this level.

5 DATA AVAILABILITY

The original gravity data from IGETS network is provided by GFZ-Potsdam at http://isdc.gfz-potsdam.de/igets-data-base/. The links to other numerical data used are provided in the text, as well as the references to adopted software. The dataset resulting from our comparative analysis is available upon request.

ACKNOWLEDGMENTS

A. Valencio thanks CNPq (Brazil) for a scholarship (process #206246/2014-5). The authors thanks the participants of the 35th General Assembly of the European Seismological Commission for the comments, and the School of Natural and Computing Sciences, University of Aberdeen, for travel support. The authors are grateful to all IGETS contributors, particularly to the station operators and to ISDC/GFZ-Potsdam for providing the original gravity data used in this study. We also thank the developers of ATLANTIDA3.1 and UTide. Part of this work was performed using the Institute for Complex Systems and Mathematical Biology High Performance Computing Cluster, University of Aberdeen.

REFERENCES

Agnew, D., 2007. Earth Tides, in *Treatise on Geophysics and Geodesy*, pp. 163–195, ed. Herring, T., Elsevier, New York.

Bezruchko, B. & Smirnov, D., 2010. *Extracting knowledge from time series: an introduction to nonlinear empirical modeling*, Springer, Berlin, Heidelberg.

Boy, J.-P. & Hinderer, J., 2006. Study of the seasonal gravity signal in superconducting gravimeter data, *Journal of Geodynamics*, **41**(1), 227–233.

Codiga, D., 2011. Unified tidal analysis and prediction using the UTide Matlab functions, Tech. rep., Graduate School of Oceanography, University of Rhode Island, Narragansett, RI.

Crossley, D. & Hinderer, J., 2009. A review of the GGP network and scientific challenges, *Journal of Geodynamics*, **48**(3-5), 299–304.

Crossley, D., Hinderer, J., & Riccardi, U., 2013. The measurement of surface gravity, *Reports on Progress in Physics*, **76**(4), 046101.

Darwin, G.H., 1907. *Scientific Papers: sir George Howard Darwin, v.1*, Cambridge University Press, Cambridge.

Dierks, O. & Neumeyer, J., 2002. Comparison of Earth Tides Analysis Programs, *Bulletin d'Informations Mareés Terrestres*, **135**, 10669–10688.

Farrell, W., 1972. Deformation of the Earth by Surface Loads, *Reviews of Geophysics and Space Physics*, **10**(3), 761–797.

Farrell, W., 1973. Earth Tides, Ocean Tides and Tidal Loading, *Philosophical Transactions of the Royal Society of London A*, **274**(1239), 253–259.

Goodkind, J. M., 1999. The superconducting gravimeter, *Revi. Sci. Instrum.*, **70**(11), 4131–4152.

Hinderer, J., Crossley, D., & Warburton, R., 2015. Superconducting Gravimetry, in *Treatise on Geophysics*, pp. 59–115.

Imanishi, Y., 2004. A Network of Superconducting Gravimeters Detects Submicrogal Coseismic Gravity Changes, *Science*, **306**(5695), 476–478.

Imanishi, Y., Kokubo, K., & Tatehata, H., 2006. Effect of underground water on gravity observation at Matsushiro, Japan, *Journal of Geodynamics*, **41**(1-3), 221–226.

Imanishi, Y., Nawa, K., & Takayama, H., 2013. Local hydrological processes in a fractured bedrock and the short-term effect on gravity at Matsushiro, Japan, *Journal of Geodynamics*, **63**, 62–68.

Kantz, H. & Schreiber, T., 1997. *Nonlinear Time Series Analysis*, Cambridge University Press, Cambridge.

Merrian, J., 1992. Atmospheric pressure and gravity, *Geophysical Journal International*, **109**, 488–500.

Montagner, J.-P., Juhel, K., Barsuglia, M., Ampuero, J. P., Chassande-Mottin, E., Harms, J., Whiting, B., Bernard, P., Clévédé, E., & Lognonné, P., 2016. Prompt gravity signal induced by the 2011 Tohoku-Oki earthquake, *Nature Communications*, **7**, 13349.

Peterson, J., 1993. Observations and modelling of background seismic noise, Tech. rep., USGS, Albuquerque, NM.

Sato, T., Okuno, J., Hinderer, J., MacMillan, D. S., Plag, H. P., Francis, O., Falk, R., & Fukuda, Y., 2006. A geophysical interpretation of the secular displacement and gravity rates observed at Ny-Ålesund, Svalbard in the Arctic - Effects of post-glacial rebound and present-day ice melting, *Geophysical Journal International*, **165**(3), 729–743.

Scragle, J., 1982. Studies in astronomical time series analysis. II. Statistical aspects of spectral analysis of unevenly spaced data, *The Astrophysical Journal*, **263**, 835–853.

Soldati, G., Piersanti, A., & Boschi, E., 1998. Global postseismic gravity changes of a viscoelastic Earth, *Journal of Geophysical Research*, **103**(12), 19,819–867,885.

Spiridonov, E., Vinogradova, O., Boyarskiy, E., & Afanasyeva, L., 2015. Atlantida3.1_2014 for Windows: a software for tidal prediction, *Bulletin d'Informations Mareés Terrestres*, **149**, 12062–12081.

Tamura, Y., 1987. A Harmonic Development of the Tide-Generating Potential, *Bulletin d'Informations Mareés Terrestres*, **99**, 6813–6855.

Tamura, Y. & Agnew, D. C., 2008. *Baytap08 User's Manual*.

Van Camp, M., de Viron, O., Pajot-Métivier, G., Casenave, F., Watlet, A., Dassargues, A., & Vanclooster, M., 2016. Direct measurement of evapotranspiration from a forest using a superconducting gravimeter, *Geophysical Research Letters*, **43**(19), 10,225–10,231.

Venedikov, A., Arnoso, J., & Vieira, R., 2001. Program VAV-2000 for Tidal Analysis of Unevenly Spaced Data with Irregular Drift and Colored Noise, *Journal of the Geodetic Society of Japan*, **47**(1), 281–286.

Wahr, J., 1985. Deformation induced by polar motion, *Journal of Geophysical Research*, **90**(B11), 9363–9368.

Wenzel, H., 1996. The nanogal software: Earth tide data processing package ETERNA 3.30, *Bulletin d'Informations Mareés Terrestres*, **124**, 9425–9439.

Supplementary Material

On the results Section, Fig. 4 provided the power spectral density of the original signal and the gravity residuals obtained from the different methods for the BF1 station, Schiltach/Black Forest, Germany. Figures (A1–A7) here in the Supplementary Material present the resulting plots for the same analysis in the remaining stations.

Comparing the procedures for tidal removal, it should be noted in all cases the distortion of the spectrum after the procedures of frequency filtering. In the case of Fourier filtering, the frequency gaps related to removed tides are significant, implying in considerable bandwidths unavailable from geophysical analysis, and artificial loss of information for physical applications. The case of FIR filtering maintained for most stations the terdiurnal tides (around $3.5 \cdot 10^{-5}$ Hz) and the overall frequency spectrum usually present distortions most evident around $0.5 \cdot 10^{-5}$ Hz and $4.4 \cdot 10^{-5}$ Hz. The considerable peaks in diurnal (around $1.16 \cdot 10^{-5}$ Hz) and especially semidiurnal (around $2.31 \cdot 10^{-5}$ Hz) bands in the residuals from physical modelling indicate present-day challenges in the theoretical description of the Earth system. These residuals can vary considerably with location, depending on how well the theoretical model reflects the local environment. Particular challenges are shown at the SU stations (Sutherland, South Africa). The data-based modelling reflects an improvement compared to physical modelling, as the largest diurnal and semidiurnal amplitudes have reduced, but tides remain present. The background noise level is being lowered in amplitude in the modelling procedures compared to the filtering methods. As a results it is possible to observe the quaterdiurnal tides (around $4.63 \cdot 10^{-5}$ Hz) in most stations using the modelling methods.

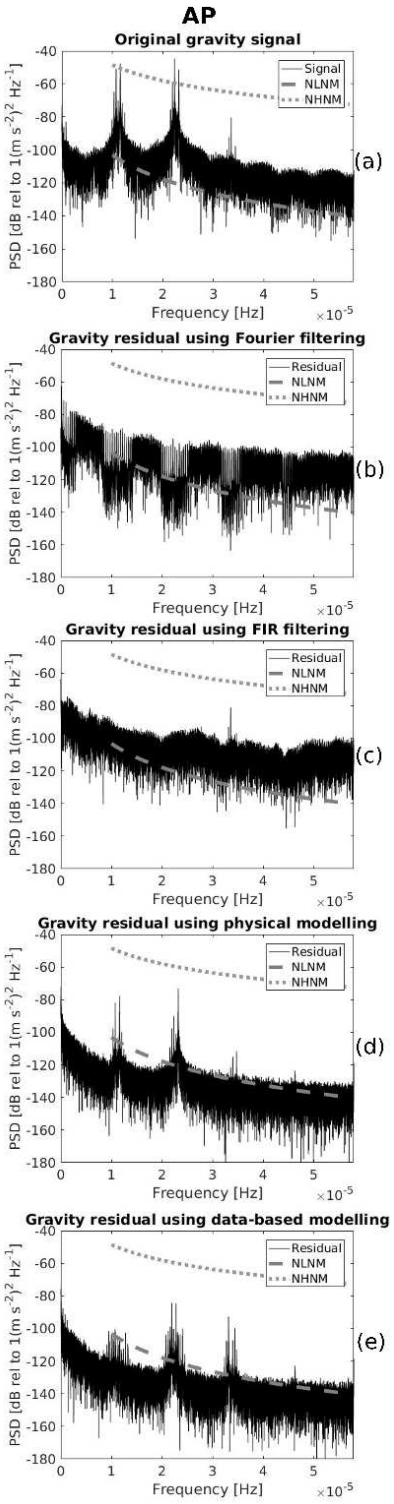

Figure A1. Lomb-Scragle power spectral density of the original gravity signal (a) and gravity residuals (b-e) from AP instrument, Apache Point (New Mexico). New Earth Low Noise (NLNM) and High Noise Models (NHNM) are indicated.

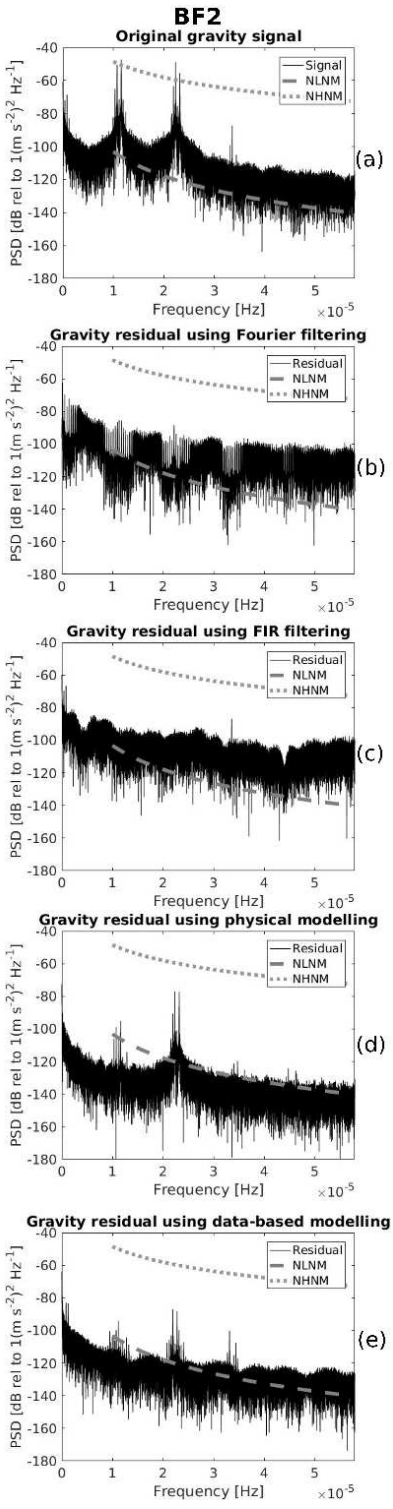

Figure A2. Lomb-Scragle power spectral density of the original gravity signal (a) and gravity residuals (b-e) from BF2 instrument, Schiltach/Black Forest (Germany). New Earth Low Noise (NLNM) and High Noise Models (NHNM) are indicated.

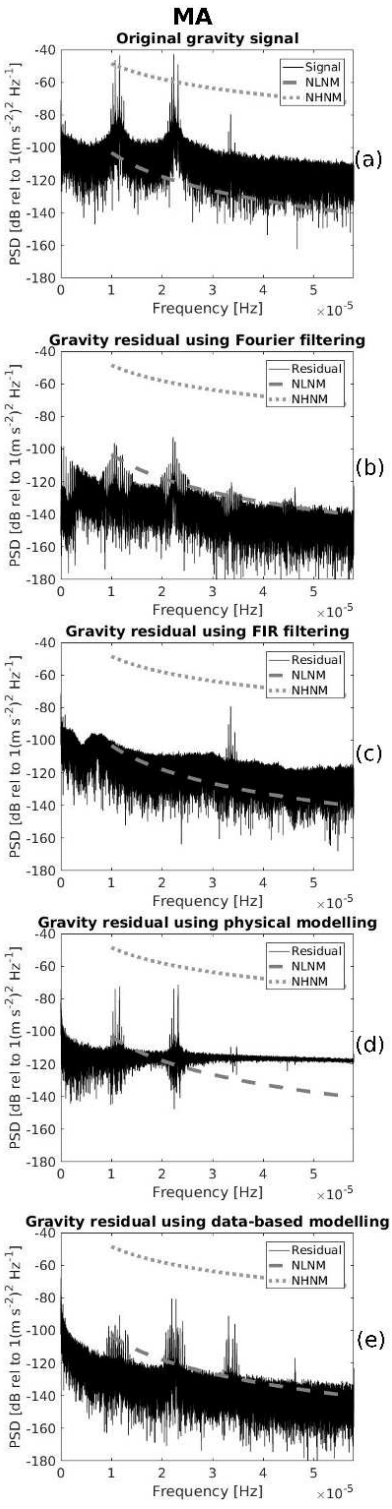

Figure A3. Lomb-Scragle power spectral density of the original gravity signal (a) and gravity residuals (b-e) from MA instrument, Matsushiro (Japan). New Earth Low Noise (NLNM) and High Noise Models (NHNM) are indicated. The sharpening of the noise spectrum above $2.5 \cdot 10^{-5}$ Hz in (d) is an artificial effect of the Lomb computation. Only the presence of peaks should be considered in this case.

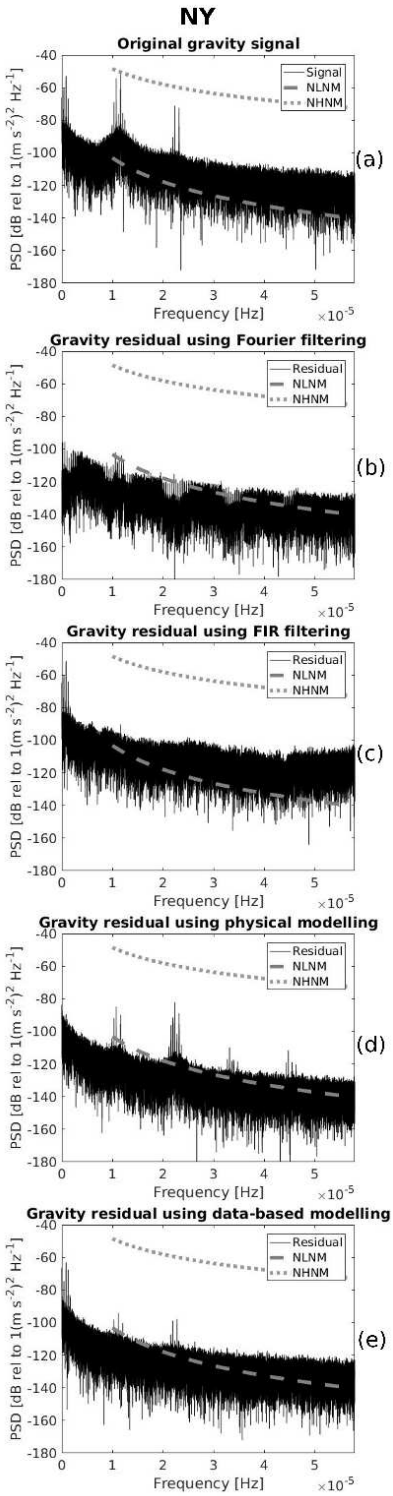

Figure A4. Lomb-Scragle power spectral density of the original gravity signal (a) and gravity residuals (b-e) from NY instrument, Ny-Ålesund (Svalbard island, Norway). New Earth Low Noise (NLNM) and High Noise Models (NHNM) are indicated.

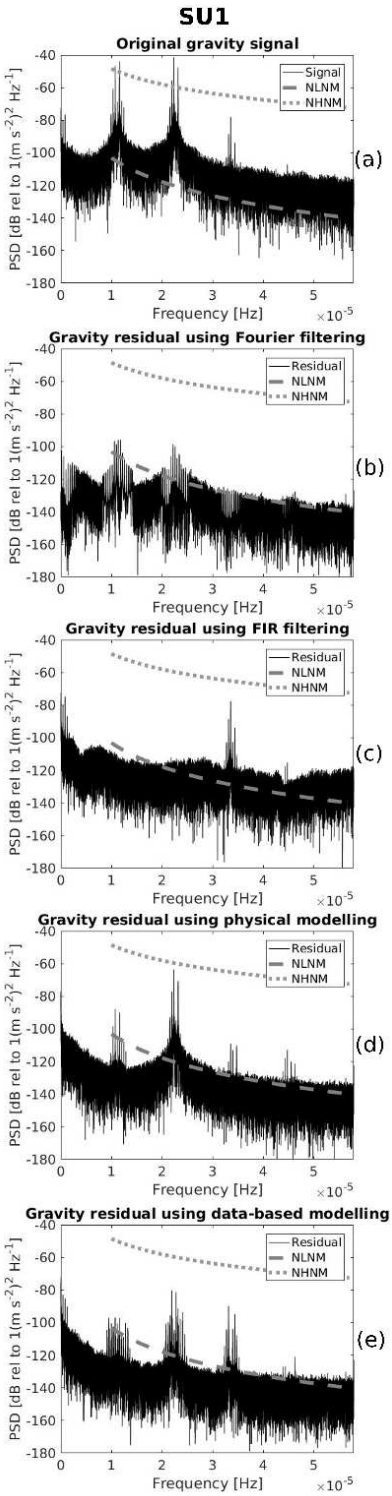

Figure A5. Lomb-Scragle power spectral density of the original gravity signal (a) and gravity residuals (b-e) from SU1 instrument, Sutherland (South Africa). New Earth Low Noise (NLNM) and High Noise Models (NHNM) are indicated.

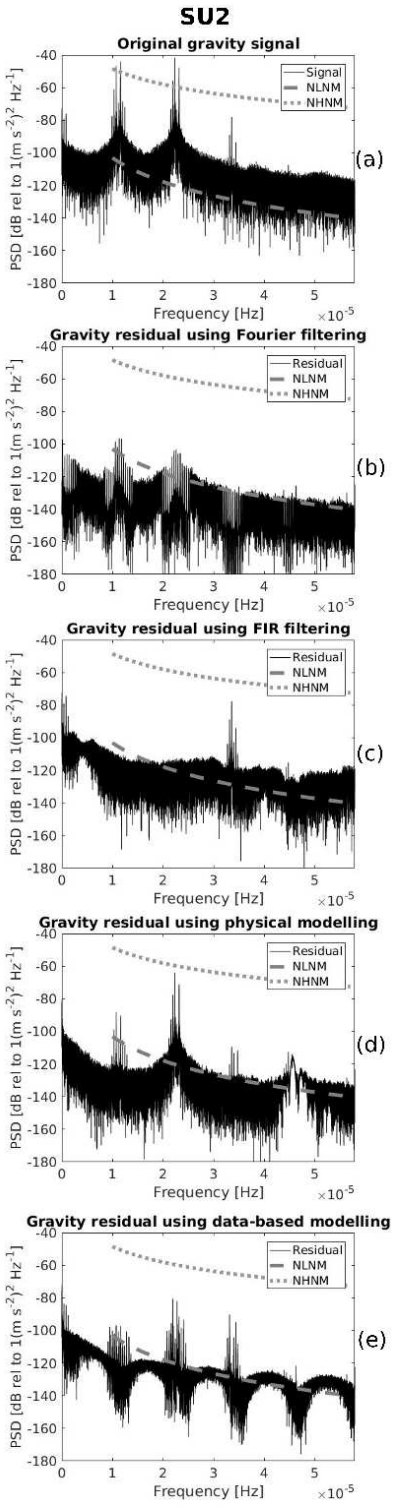

Figure A6. Lomb-Scragle power spectral density of the original gravity signal (a) and gravity residuals (b-e) from SU2 instrument, Sutherland (South Africa). New Earth Low Noise (NLNM) and High Noise Models (NHNM) are indicated. The fluctuations in the background noise in (e) are artificial effects of the Lomb computation, analogous to the windowing effects in regular periodograms. Only the presence of peaks should be considered in this case.

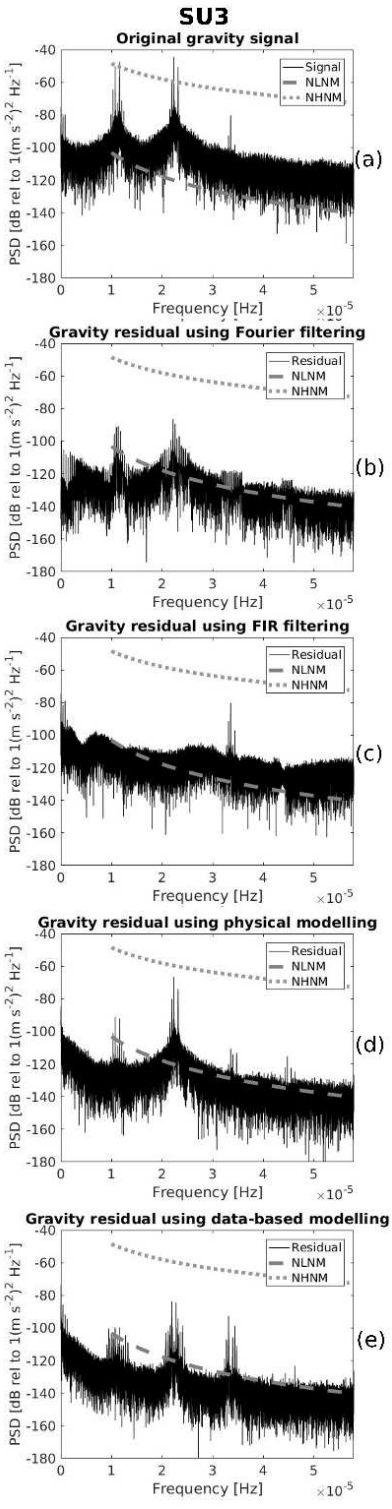

Figure A7. Lomb-Scragle power spectral density of the original gravity signal (a) and gravity residuals (b-e) from SU3 instrument, Sutherland (South Africa). New Earth Low Noise (NLNM) and High Noise Models (NHNM) are indicated.